Evaluating Statistical Versus Deterministic Imaging Strategies for Cluttered Near-Surface Models

Andrey Bakulin[1], Maxim Protasov[2(✉)], Ilya Silvestrov[3], Dmitry Neklydov[2], Maxim Dmitriev[4], and Denis Sabitov[5]

[1] Bureau of Economic Geology, University of Texas at Austin, Austin, USA
[2] Institute of Petroleum Geology and Geophysics, 3, Koptuga Street, Novosibirsk 630090, Russia
protasovmi@ipgg.sbras.ru
[3] PGS Kazakhstan, Almaty, Kazakhstan
[4] EXPEC Advanced Research Center, Saudi Aramco, Dhahran 31311, Saudi Arabia
[5] Aramco Innovations LLC, Saudi Aramco, Moscow 117105, Russia

Abstract. In the paper we consider complex land near surface modeled as random clutter, and we study the depth imaging problem for such media. We consider synthetic clutter models, and we provide a numerical study using various realizations of the cluttered models. We propose and investigate a statistical imaging technique based on path summation allowing to get depth image without reconstruction of deterministic near-surface depth velocity model. Our results demonstrate that statistical imaging can significantly improve and recover reflectors, even with a limited number of realizations. The ability to achieve accurate images despite the absence of an exact velocity model underscores the robustness of this technique. We show that statistical imaging can average out phase distortions caused by near-surface clutter, enhancing the clarity and accuracy of the subsurface image. This method offers a promising direction for imaging in complex near-surface environments, effectively addressing the limitations of traditional deterministic approaches. We further explain why this technique works by leveraging the concept of "seismic speckle," analogous to optical and ultrasonic speckle noise, to account for phase distortions caused by small-scale heterogeneities. By estimating the statistical properties of the clutter, we generate ensembles of velocity models that perturb the phase of the depth-migrated arrivals symmetrically. In summary, our study highlights the potential of statistical imaging with path summation to significantly improve seismic imaging in challenging near-surface environments, offering a robust alternative to traditional deterministic methods and paving the way for future advancements in subsurface imaging.

Keywords: Statistical imaging · Clutter · Complex Near-surface

© The Author(s), under exclusive license to Springer Nature Switzerland AG 2025
O. Gervasi et al. (Eds.): ICCSA 2025, LNCS 15648, pp. 396–414, 2025.
https://doi.org/10.1007/978-3-031-97000-9_25

1 Introduction

In the field of land seismic exploration, the quality of depth seismic images is significantly compromised by strong scattering from small- and medium-scale near-surface heterogeneities [1, 2]. These heterogeneities not only obscure deep geological structures but also introduce substantial phase errors through imperfections in the migration velocity model, which impede accurate focusing of the extrapolated wavefield [2]. Given the impracticality of reconstructing all near-surface complexities with current technology, an effective alternative treats the near-surface as a stochastic medium [3]. This approach leverages the statistical properties of the medium, enabling imaging algorithms to better address near-surface and overburden challenges, thus enhancing the accuracy of deep reflection images. Historically, several methodologies have embraced this statistical perspective. Borcea et al. advocated for an interferometric imaging technique utilizing the concept of time-reversed wave propagation to yield statistically stable images in random media [4]. Extending this, Sava and Poliannikov improved imaging quality in environments with rapid, small-scale velocity variations by modifying conventional cross-correlation migration conditions [5]. A notable shift away from reliance on precise velocity models was proposed by Landa et al. [6], who introduced a path-integral summation concept. This method aggregates images derived from a spectrum of possible velocity distributions, rather than selecting a single "optimal" model. It incorporates weighted summation to highlight the most likely aspects of the image, enhancing the reliability of the output. Path-integral imaging has found various applications in the time domain, such as stack to zero offset [7–9], time migration [6], velocity analysis [10, 11], and diffraction imaging [12]. Advancing these concepts into depth imaging poses greater challenges, necessitating careful sampling of the complex, multidimensional space of possible depth velocity models and selecting appropriate weighting functions for effective summation. Preliminary findings on the applicability of path-integral imaging in depth settings were shared in [6], demonstrating its potential for imaging beneath salt structures without precisely delineating salt-sediment boundaries [13].

Our study discovers and shows the new possibilities of statistical imaging with path summation to significantly improve seismic imaging of target deep reflectors in the presence of a challenging complex near-surface scattering layer characterized as a statistical cluttered medium whose properties should be pre-estimated.

2 Construction Realistic Model with Complex Near-Surface

2.1 Near-Surface Clutter Model: A Focus on Geological Heterogeneities

In seismic imaging, the accurate modeling and imaging of subsurface features are greatly challenged by the scale of geological heterogeneities. These variations in size critically influence how seismic waves scatter, significantly impacting the quality of subsurface imaging. Isolated heterogeneities can create localized disturbances, but a widespread distribution throughout the near-surface horizons leads to pronounced image degradation, demonstrating the profound effect of these heterogeneities [1, 2].

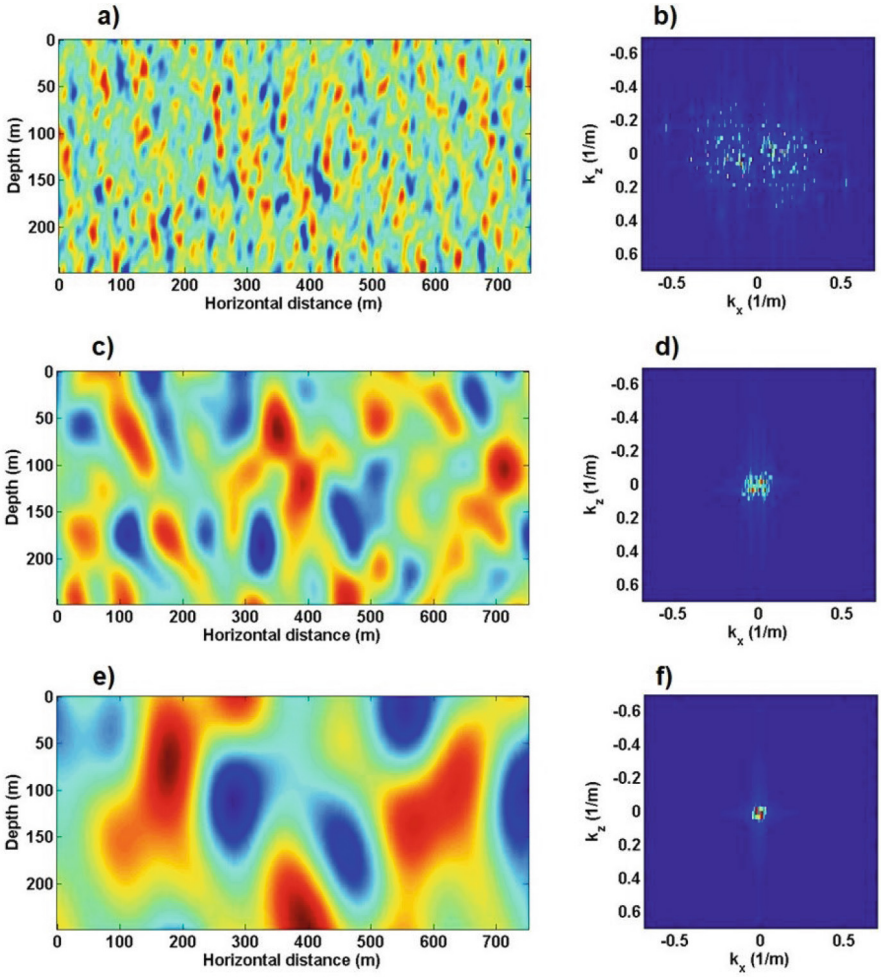

Fig. 1. Near-surface clutter models and corresponding spatial spectra for varying correlation lengths: (a, b) 10 m representing small-scale heterogeneities, (c, d) 35 m for intermediate-scale heterogeneities, and (e, f) 75 m for large-scale heterogeneities.

To assess their impact, we employ a statistical approach within a cluttered near-surface model. This model combines either a homogeneous or smoothly layered background with a random perturbation field derived using Gaussian distribution functions. Key parameters such as correlation length and standard deviation define the scale and magnitude of velocity perturbations, respectively. We illustrate this with example correlation lengths of 10 m, 35 m, and 75 m, each highlighting distinct challenges and impacts on seismic imaging as demonstrated in Fig. 1.

Seismic data typically covers a broadband range of 5–80 Hz, interacting with heterogeneities in various scattering regimes [14] determined by the normalized wave number k·a, where a is the radius of the heterogeneity and k is the wavenumber $k = 2\pi/\lambda$)):

- Effective medium ($k \cdot a < 0.01$), where scattering is negligibly small.
- Rayleigh scattering ($0.01 \leq k \cdot a < 0.1$), with low contrast of the elastic parameters, can be described using the Born approximation.
- Resonance scattering ($0.1 \leq k \cdot a < 10$), scatterer size, and wavelength have the same order. The incident waves are scattered with large angles, and a reflection coda can be observed in the wave field.
- Geometric ray theory ($10 \leq k \cdot a$), the wavelength is small compared to the scatter size. Focusing, diffraction, and interference effects become important.

While larger-scale features such as 75 m are usually within the recovery range of current velocity model building practices and fall predominantly into the geometric ray theory scattering regime, the intermediate scale of 35 m presents substantial challenges due to resonance scattering. This complicates both velocity model construction and seismic imaging. The smallest scale of 10 m often evades traditional velocity model detection, challenged by both Rayleigh and resonance scattering, further contributing to imaging challenges caused by inaccurate velocities.

Geological heterogeneity varies significantly in scale, from large to small, and in certain geological contexts like carbonate strata buildups, a dominant scale can prevail. Our numerical experiments focus on the 35 m scale heterogeneities, representing a critical threshold that starts to replicate real imaging challenges from complex settings. By concentrating on this intermediate scale, we aim to use it as a benchmark to measure progress in imaging techniques under complex near surface.

This study aims to enhance the clarity and accuracy of subsurface images produced, providing a more reliable interpretation of seismic data where these medium-scale heterogeneities dominate. Our objective is not only to push the boundaries of current imaging technology but also to refine our approaches for a better understanding of the complex interplays at work in challenging seismic settings.

2.2 Complete Seismic Model for Imaging Evaluation

In our study, we developed a comprehensive near-surface model enhanced with random clutter, illustrated in Fig. 2a. This model integrates a velocity perturbation field defined by a Gaussian distribution, where the correlation length and standard deviation—35 m and 400 m/s, respectively—specify the heterogeneity scale and velocity perturbation magnitude. Our base model maintains a homogeneous velocity of 2000 m/s. The near-surface layer is bounded to approximately 350 m depth, below which the deeper subsurface is represented by layered media with four flat reflectors. The first reflector marks the bottom of the near-surface layer.

This methodological choice to select a simplified subsurface model allows us to easily evaluate imaging disruptions caused by the complex near-surface conditions. It also mirrors the geological steps of complex desert environments in the Middle East, characterized by ‘layer cake’ geology coupled with a complex near-surface that often presents challenging imaging scenarios.

To facilitate imaging exercises and evaluation, we generated synthetic seismic data using acoustic finite-difference modeling, based on the exploding reflector concept. This approach is designed to mimic real seismic challenges, replicating the complex scattering

distortions typically observed in field data [1]. The resulting synthetic dataset provides a robust framework for testing and comparing the efficacy of different imaging strategies under realistic conditions (Fig. 2b).

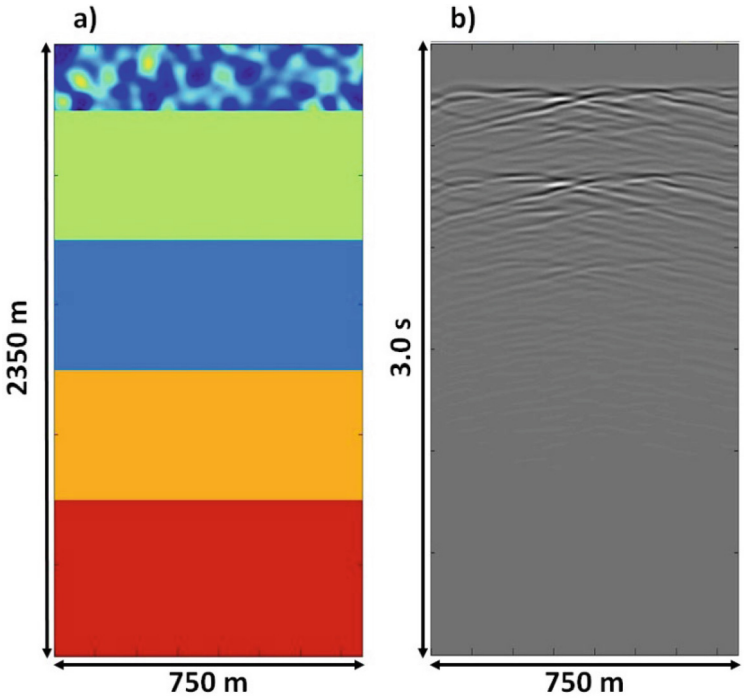

Fig. 2. (a) True model representation: complex near-surface simulated with a fixed clutter realization, featuring a spatial correlation length of 35 m, mean velocity of 2000 m/s, and a standard deviation of 400 m/s. (b) Zero-offset seismic data computed from the true model in (a). This figure illustrates the impact of near-surface complexity on seismic data, showing how small-scale heterogeneities influence the recorded wavefield.

3 Deterministic Imaging

We provide the ideal image result which is got via convolution of the true model reflectivity and the source impulse (Fig. 3a). Then we compute zero-offset data and in the true clutter model we provide reverse-time migration (RTM), the results are shown in Fig. 3b. This RTM result contains numerous imaging artifacts alongside the true subsurface reflectors. For benchmarking purposes, the ideal image is used as the exact reference solution and the image obtained from the true clutter model is used as the best achievable result.

Next we provide a realistic imaging scenario, where we know the initial smooth "tomographic" velocity model (Fig. 4a) that approximates the true model but lacks

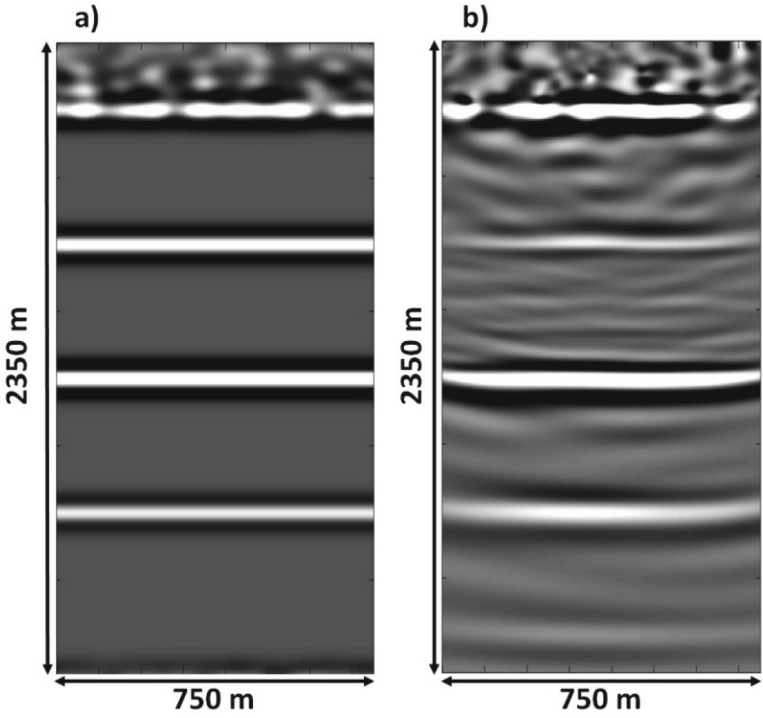

Fig. 3. (a) True model reflectivity used as the ideal image reference. (b) Zero-offset RTM image in the true clutter model, representing the best achievable migrated image. Although the best achievable image still has many artifacts, it proves that migration can produce great images if all velocity details, including small-scale heterogeneities, are accurately recovered.

many smaller details. We further assume, without proof, that the perturbations between the background and true model follow a Gaussian distribution. We estimate the two parameters of this distribution directly from the data, with the correlation length kept at 35 m and the standard deviation reduced to 257 m/s. This standard deviation is based on the difference between the smooth "tomographic" and the true clutter models.

Using these statistical parameters allows for the efficient generation of an ensemble of models. Figure 3b shows one such model realization. We then applied conventional deterministic imaging to both the smooth model and the detailed model, which is one realization with pre-defined clutter parameters. The migration results for both the smooth clutter model and any model realization yield defocused images (Fig. 4a, 4b), with only parts of the reflected interfaces being properly migrated.

Our tests indicate that conventional deterministic imaging can yield appropriate results when the model is known exactly. However, medium- and small-scale features pose significant challenges, and conventional velocity model building is imperfect, making this approach often difficult to achieve optimal results.

When only a smooth background velocity model is available, deterministic imaging struggles to produce satisfactory images. Even with detailed knowledge of clutter parameters, this approach cannot consistently generate models that deliver reliable results. This highlights the need for alternative imaging strategies that can better handle the complexities introduced by near-surface heterogeneities (Fig. 5).

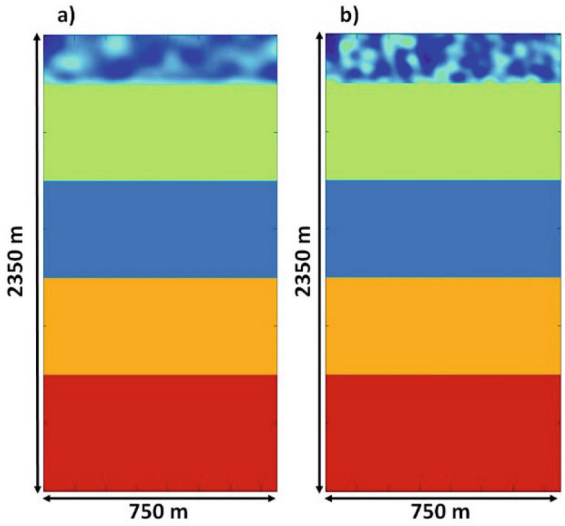

Fig. 4. (a) Smooth background model of the true clutter, assumed to be recovered during conventional velocity model building. (b) A single realization of the model generated by introducing Gaussian perturbations to the smooth model from (a), with a correlation length of 35 m and a standard deviation of 257 m/s for the perturbations. This comparison highlights the differences between a conventional smooth model and a perturbed realization, illustrating the potential impact of small-scale heterogeneities on seismic imaging.

4 Statistical Imaging

4.1 Path Summation

Instead of relying on the uncertain reconstruction of an exact velocity model [2], the path-summation method generates multiple realizations of the depth model [6] that could capture accurate fragments of the depth velocity model. The final image is a weighted summation of these elementary images constructed for every model realization, allowing each one to contribute valuable pieces to the overall picture.

In our case, imaging in a desert environment with a complex near-surface is achieved by summing individual migrated images computed for different realizations of the near-surface migration velocity model as follows:

$$I_w(x) = \sum\nolimits_k w_k(x) I_k(x) \tag{1}$$

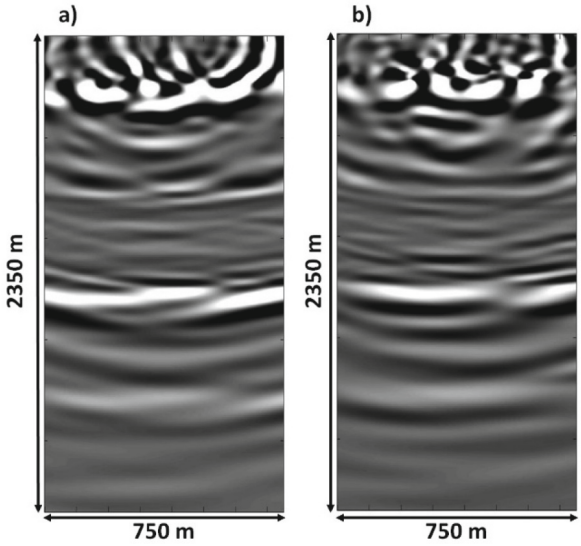

Fig. 5. Zero-offset images obtained with different velocity models: (a) smooth background model shown in Fig. 4a; (b) single realization from the clutter ensemble shown in Fig. 4b. Both images struggle to focus subsurface reflectors, highlighting the challenges posed by near-surface heterogeneities on imaging accuracy.

where I_w is a final image at point x, I_k is the image for model realization with k, and w_k is a weighting function, which is set to 1 in this study. This procedure can be viewed as statistical averaging over an ensemble of possible near-surface models.

We define the near-surface model realizations using statistical modeling of random anomalies, known as clutter. Given that the scale of the anomalies of interest is comparable to or smaller than the dominant source wavelength, we use reverse-time migration (RTM) to accurately address them during wave propagation. For simplicity, we consider post-stack RTM in this work, though the results can be extended to the case of pre-stack migration.

4.2 Statistical Imaging Investigation

To investigate statistical imaging using the path summation approach, we start with a smooth "tomographic" near-surface model as a reference solution (Fig. 4a). We assume a correlation length of 35 m and define the standard deviation as 257 m/s, based on the difference between the true clutter and the "tomographic" model.

We generated 100 model realizations and performed zero-offset RTM migration for each, resulting in 100 images. Images for three different model realizations are shown in Fig. 6. Finally, we applied the path summation approach to this scenario. Traces for fixed horizontal positions for all 100 images are presented in Fig. 7, where fluctuations of the events near the true reflector positions can be observed.

These images were stacked using simple summation (1). The migration result for individual realizations generally provides defocused images (Fig. 6), with only some parts of the reflected interfaces properly migrated. However, even a simple summation results in a stacked image that shows reflected events over most of the area (Fig. 8a).

By performing migration with different models of the same data, we can generate an analog of a common-image gather (CIG) of RTM zero-offset migration with respect to the model realizations (Fig. 7). These raw CIGs do not provide flat events at the reflector positions; instead, they are scattered due to the different perturbations in the clutter realizations.

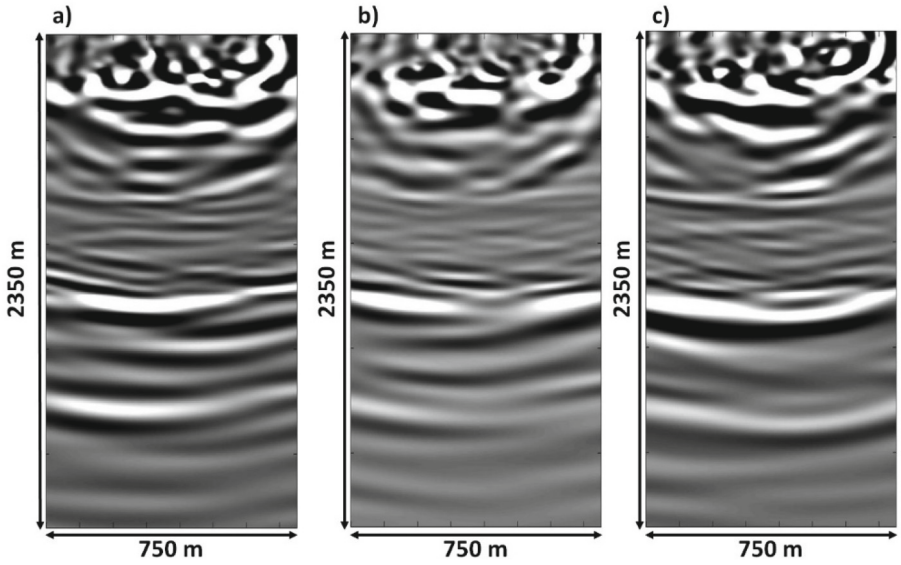

Fig. 6. Zero-offset RTM images obtained from three different single realizations of the clutter ensemble used in statistical imaging. These images demonstrate the variability and phase distortions caused by different near-surface clutter realizations, showcasing the challenges in achieving accurate seismic imaging without statistical averaging.

Next, we investigate the influence of the number of realizations on the statistical imaging result. We compute simple stacks with different numbers of iterations: 5, 10, 25, 50, and 100 (Fig. 9). Visually, it is challenging to judge qualitatively which stack image is better. Therefore, we use two quantitative measures: signal-to-noise ratio (SNR) and correlation coefficient. Both measures use standard definitions and utilize the ideal image result (Fig. 9a) as the reference.

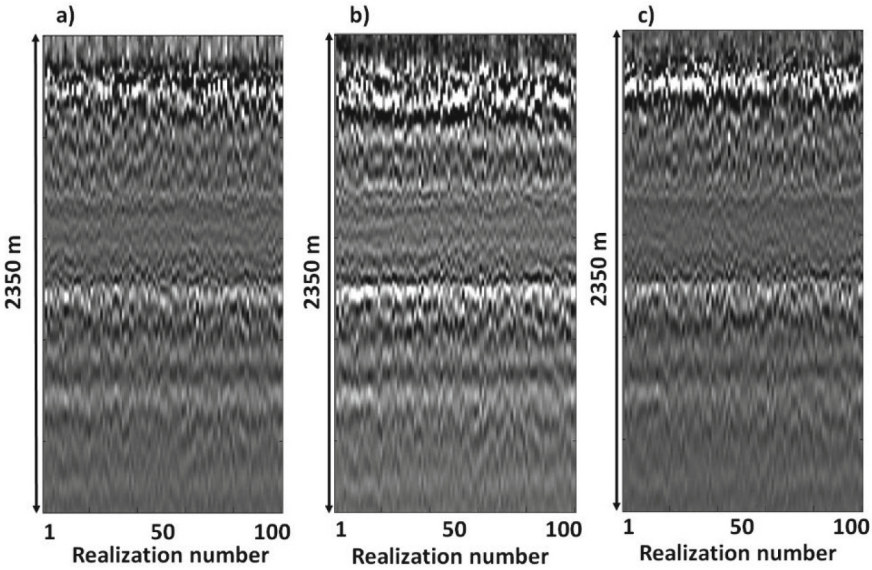

Fig. 7. Common-image gathers of zero-offset migration with respect to the model realizations at three different horizontal positions: (a) x = 250 m; (b) x = 375 m; (c) x = 500 m. These gathers illustrate the variability in the seismic reflections due to different realizations of the near-surface model, highlighting the phase distortions and amplitude variations across different locations.

We compute SNR values and correlation coefficients for the entire images and for the image parts containing reflected interfaces near 750 m, 1250 m, and 1750 m. Analyzing the results in Table 1, it is evident that the image obtained from the true clutter model is the best achievable solution, despite appearing noisier than the path summation weighted images.

Additionally, all path summation results provide better solutions than any single realization. Notably, the SNR and correlation coefficient values for the simple stacks with 10, 25, 50, and 100 iterations are very close. This indicates that only a few realizations are needed in statistical imaging to achieve a sufficiently good solution.

Next, we investigate the influence of errors in the statistical parameters of the clutter on the results of statistical imaging. We introduce different levels of error in the values for the standard deviation and correlation lengths: -15%, $+15\%$, and $+50\%$. The statistical image results for clutters with these errors are presented in Fig. 10.

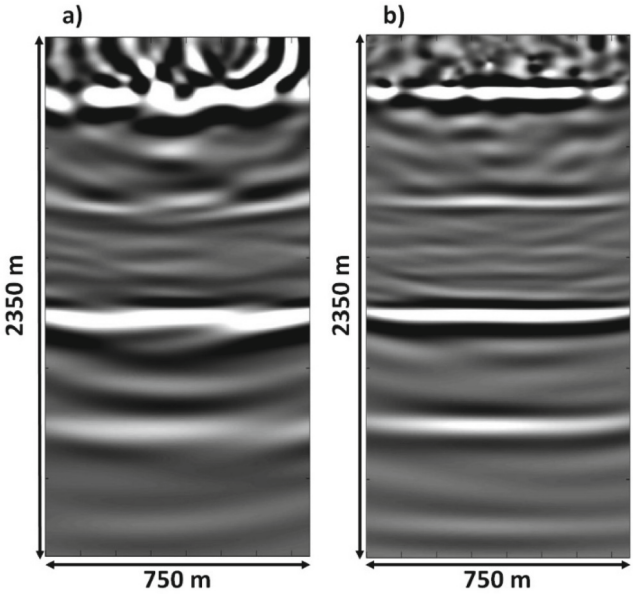

Fig. 8. Comparison of statistical image and best achievable migrated image: (a) statistical image obtained using simple stack path summation; (b) zero-offset RTM image in the true clutter model, representing the best achievable migrated image. This figure illustrates the effectiveness of statistical imaging with path summation compared to the best achievable result using the true clutter model. The statistical image in (a) demonstrates how path summation can approximate the ideal migration outcome shown in (b), despite the absence of the exact velocity model.

Visually, the statistical images for errors of -15% and $+15\%$ are close to the images obtained with the correct clutter parameters. However, the statistical images for a 50% error significantly differ from those obtained with true values. For a quantitative comparison, we compute SNR values and correlation coefficients, summarizing the results in Table 2. The quantitative and visual comparisons lead to similar conclusions: statistical imaging provides stable results concerning clutter parameters, which is crucial for its practical application.

5 Why Statistical Imaging Works?

Inspired by studies of optical and ultrasonic speckle noise [15], we hypothesize that seismic data experiences similar distortions caused by near-ballistic forward scattering of multiple arrivals. We refer to this phenomenon as "seismic speckle" [16]. Speckle is typically modeled as multiplicative noise. Analogously, we can interpret image distortions after depth migration of such data. To illustrate this, we provide an analogy for common-image gathers obtained from different model realizations. Let us describe the seismic trace model incorporating general multiplicative noise. The image trace for the k-th realization is represented as:

$$i_k(z) = r_k(z) * s(z) + n_k(z), \tag{2}$$

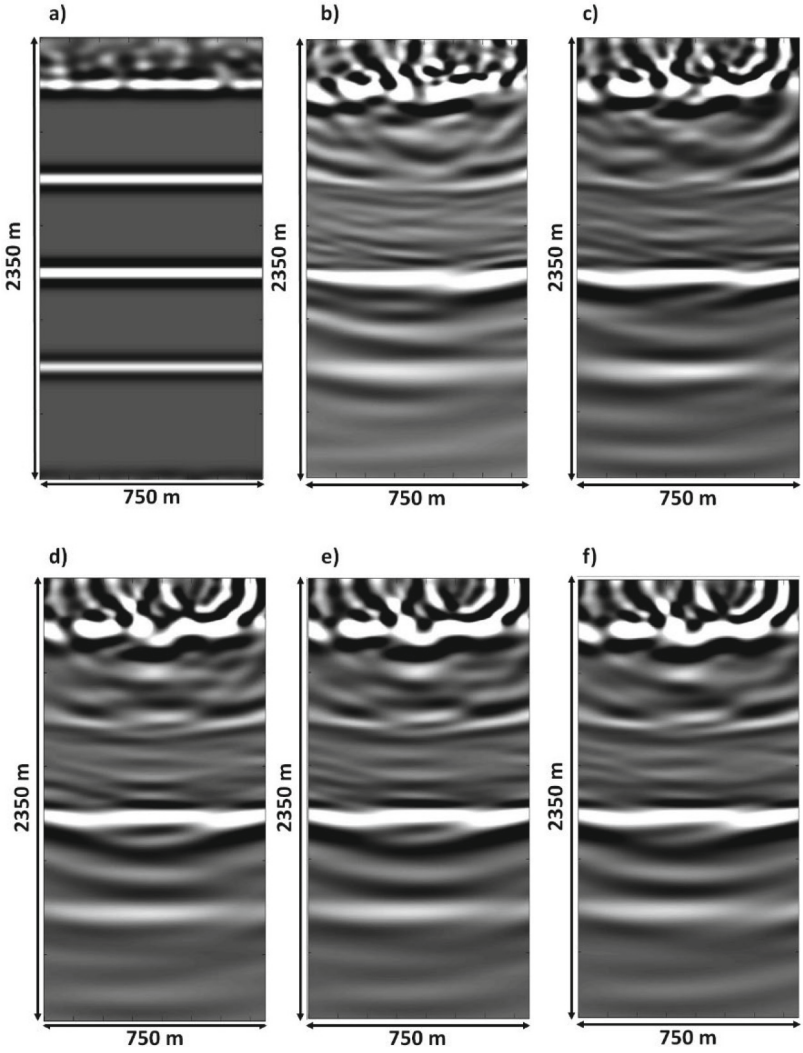

Fig. 9. Effect of number of realizations on statistical imaging: (a) True model reflectivity: ideal image reference; (b)–(e) Statistical images with varying number of realizations: (b) 5 Realizations; (c) 10 Realizations; (d) 25 Realizations; (e) 50 Realizations. Observe that images (c)–(d) are similar, suggesting that even a small number of realizations can achieve a reasonable statistical image.

where $s(z)$ is the clean image trace, $r_k(z)$ is multiplicative noise, $n_k(z)$ is additive random noise. In the Fourier domain (2) is written as:

$$I_k(p_z) = R_k(p_z)S(p_z) + N_k(p_z), \tag{3}$$

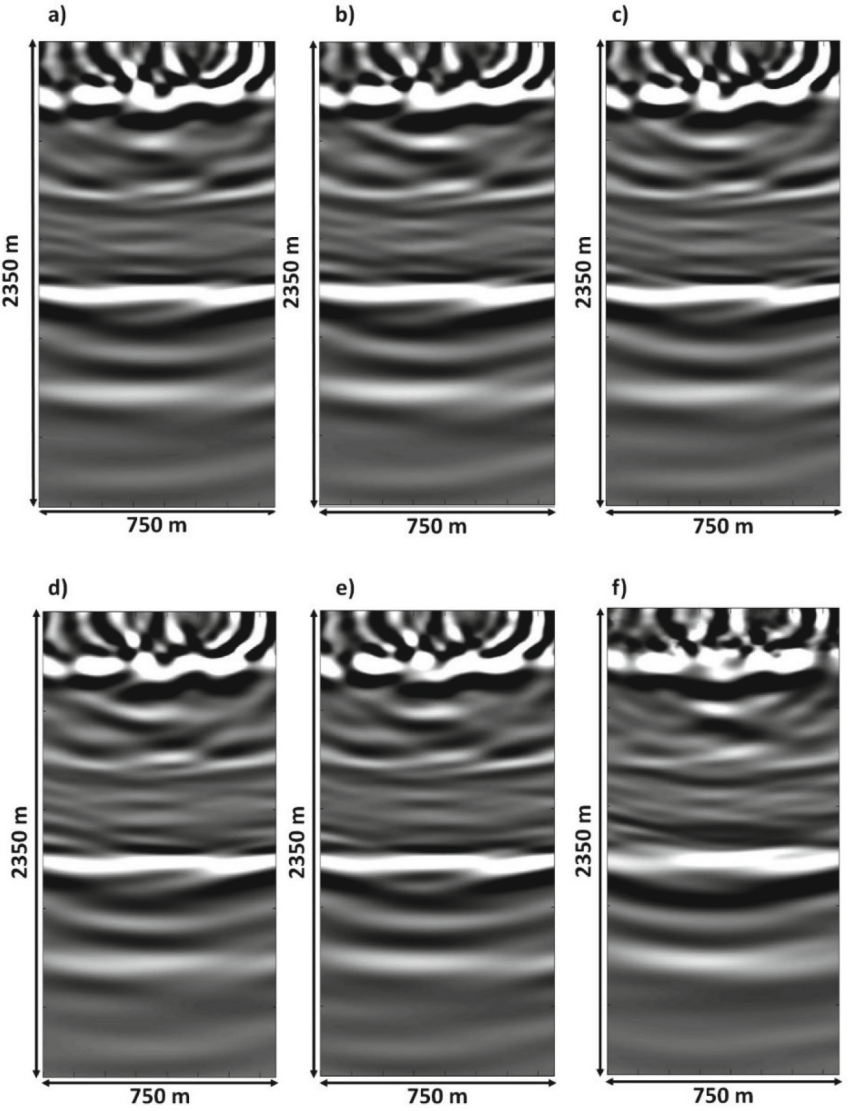

Fig. 10. Statistical images obtained with path summation using simple stacking for different clutter parameters: (a) correct; (b) standard deviation error +15%; (c) standard deviation error −15%; (d) correlation length error +15%; (e) correlation length error −5%; (f) standard deviation error +50%, correlation length error +50%. These results demonstrate that statistical imaging is robust to small errors in clutter parameters (around ±15%) but shows significant degradation with larger errors (around ±50%). This indicates that approximate values within a certain range can still yield better images using statistical imaging, without the need for precise accuracy.

Table 1. Quality control metrics for statistical images obtained by summing different numbers of realizations, including SNR (in dB) and correlation coefficient. These metrics are computed based on quantitative comparison with the ideal image reference.

Metric	RTM in true model	Single realization	Sum of 100 realizations	Sum of 50 realizations	Sum of 25 realizations	Sum of 10 realizations	Sum of 5 realizations
SNR	3.5	−2.5	−0.7	−0.6	−0.3	−0.7	−1.7
Correlation coefficient	0.75	0.18	0.4	0.4	0.43	0.34	0.3

Table 2. Quality control metrics for images with different clutter parameters: SNR and correlation coefficient. The table evaluates the impact of estimating errors on image quality, based on comparisons with the ideal reference (true reflectivity) and the best achievable image (RTM in the true model). These results show that approximate clutter parameters are sufficient for obtaining better images, highlighting the practical applicability of statistical imaging.

Metric	RTM in true model	Stat image, no error	Stat image, std +15%	Stat image, std −15%	Stat image, cor. len. +15%	Stat image, cor. len. −15%	Stat. Image, std and cor. len. + 50%
SNR	3.5	−0.7	−0.8	−1.1	−0.4	−0.7	−1.9
Correlation coefficient	0.75	0.4	0.37	0.3	0.41	0.36	0.28

where p_z is the variable in the Fourier domain, I_k, R_k, S, N_k are Fourier transforms of the corresponding depth-domain functions,. We specify a more explicit form of multiplicative noise as a random frequency-dependent phase fluctuations occurring for each realization:

$$R_k(p_z) = e^{i\varphi_k(p_z)}. \tag{4}$$

Here φ_k is the phase of the function R_k. The local stacking result of the K traces in the frequency domain is given by

$$\widehat{S}(p_z) = \frac{1}{K}\sum_{k=1}^{K}\left\{S(p_z)e^{i\varphi_k(p_z)} + N_k(p_z)\right\}. \tag{5}$$

Since the number of traces used in the stacking process is limited, $\widehat{S}(p_z)$ would be a random variable for different trace ensembles. If random variables $\varphi_k(p_z)$ describing phase perturbations have the same distributions for each realization, then the mathematical expectation is expressed as:

$$E\left[\widehat{S}(p_z)\right] = |S(p_z)|e^{i\varphi_s(p_z)}\Phi(p_z). \tag{6}$$

Without specifying further details of the near surface and migration process, we can draw important conclusions. If phase perturbations $\varphi_k(p_z)$ follow a normal (Gaussian) distribution with zero mean and standard deviation $\sigma(p_z)$, then mathematical expectation can be expressed as

$$E\left[\widehat{S}(p_z)\right] = |S(p_z)|e^{i\varphi_S(p_z)}e^{-\frac{\sigma^2(p_z)}{2}}. \tag{7}$$

For multiplicative noise caused by random depth shifts dz_k between channels (residual static that corresponds to different reflector positions for different realizations), the form is:

$$R_k(p_z) = e^{-ip_z dz_k}. \tag{8}$$

If statics are normally distributed with zero mean and standard deviation σ_z, then

$$E\left[\widehat{S}(p_z)\right] = |S(p_z)|e^{i\varphi_s(p_z)}e^{-\frac{p_z{}^2\sigma_z^2}{2}}. \tag{9}$$

Again, the phase spectrum remains the same as the clean signal, while the amplitude experiences exponential loss with frequency. When considering both types of multiplicative, then the mathematical expectation is given by:

$$E\left[\widehat{S}(p_z)\right] = |S(p_z)|e^{i\varphi_s(p_z)}e^{-\frac{p_z{}^2\sigma_z^2}{2}}e^{-\frac{\sigma_\varphi^2}{2}}. \tag{10}$$

The phase of the mathematical expectation matches the clean signal phase, while the amplitude loss is a product of two terms: one due to phase perturbations and the other due to residual statics. These results, as presented in the paper [16] in the context of speckle noise studies, demonstrate how phase cleanup and amplitude filtering occur during stacking.

Let us now revisit the common-image gather from the described experiments (Fig. 11a) and focus on the domain around the reflector at a depth of 1250 m (Fig. 11b) to establish a connection with speckle-based considerations. The ensemble shown in Fig. 11b can be viewed as carrying an identical reference signal (fixed subsurface reflector) but disturbed by different speckle patterns created numerically through RTM imaging with random near-surface models. Analyzing the phase variation of the window from Fig. 11b at two spatial frequencies, we observe that they show a symmetric Gaussian-like distribution (Fig. 12b, c), similar to what is seen in speckle noise. Note that zero in this plot corresponds to the average phase, i.e., the phase of the statistical image after summing all realizations. The symmetry resembles the assumption of speckle noise presented above. In physical experiments, we are restricted to a single realization of the clutter. Therefore, for seismic imaging in the presence of speckle noise, the strategy has been to use nearby traces with slightly different source/receiver positions for local stacking, thereby revealing the undistorted reflector phase of the common signal reflector [16]. In our study, however, we have the luxury of numerically realizing different models and speckle patterns at one location through simulation and imaging. This allows us to systematically perturb the near-surface models and enable statistical imaging to recover a cleaned-up

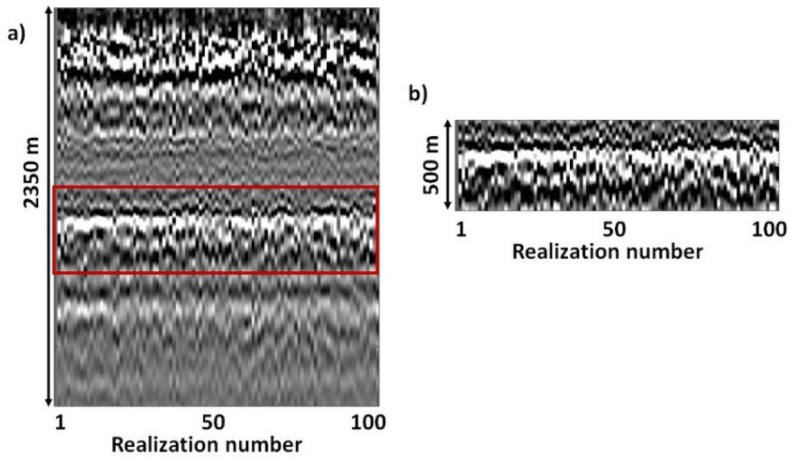

Fig. 11. (a) Common-image gather of zero-offset migration with respect to the model realizations at $x = 375$, emphasizing the impact of different near-surface clutter realizations on phase. (b) Zoomed-in view around the reflector at a depth of 1250 m, revealing an on average similar reflector disturbed by different speckle patterns created through RTM imaging with random near-surface models. The phase perturbations appear quasi-random, similar to speckle noise.

average phase in a similar way. Another similarity is that the spectrum after summation loses higher frequencies, as seen in Fig. 12a, which echoes high-frequency attenuation observed in Eq. (10). These two observations – near-symmetric phase disturbances and attenuation of higher frequencies upon stacking – establish a clear link between statistical imaging and speckle noise studies [15, 16]. These results align with the behavior predicted by formula (10), indicating that phase perturbations in the pre-summation common-image gathers could be described by the simple multiplicative model (2).

These considerations assume that our average tomographic model is a reasonable representation of the near-surface layer with small-scale heterogeneities, consistent with what is expected from seismic velocity model building, which typically yields smoothed or average velocity models. Additionally, by estimating the statistical properties of the clutter, we can generate ensembles of velocity models that perturb the phase of the depth-migrated arrivals symmetrically. Under these assumptions, the statistical collection of images before summation produces a distribution of phases that, upon stacking, can reveal the true reflector signal phase, resulting in images approaching what we would have with the true clutter model, which is unattainable in practice. The intriguing point is that each realization produces a distorted phase and image that by itself may have little value. However, their collection acquires extra power, essentially enabling them to "vote" and reveal a much more meaningful phase and image, effectively seeing through the small-scale heterogeneities. Remarkably, the actual true clutter realization that could have produced a similarly good image is not even present in the ensemble that generates the statistical image. And yet, we are able to get a robust image approaching one obtained with the true model. The initial price to pay for this improvement is that statistical images are likely to contain lower frequencies compared to the initial ones, as higher frequencies

are more prone to attenuation upon stacking. However, finding those crisper and less distorted reflections in images, even at lower frequencies, holds promise. This could potentially allow the recovery of higher frequencies in the future, making this approach a hopeful aspiration for further work despite its current limitations.

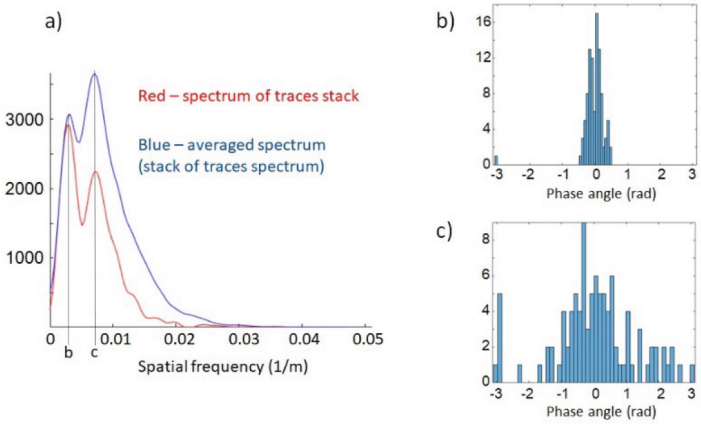

Fig. 12. (a) Amplitude spectra of common-image gather traces before and after summation, illustrating the attenuation of higher frequencies after summation—a characteristic effect of averaging multiple realizations impacted by speckle noise. (b), (c) Histograms of phase angle fluctuations for two peak frequencies, highlighting the quasi-random nature of phase perturbations. These histograms demonstrate a near-symmetric Gaussian-like distribution of phase angles around the average phase, aligning with the behavior predicted by the multiplicative model of random speckle noise.

6 Conclusions

In this study, we applied statistical imaging with path summation to synthetic land data characterized by a complex near-surface modeled as random clutter. Our findings demonstrate that near-surface clutter significantly degrades reflection images if not properly accounted for. While migration using the exact velocity model of the clutter can recover reflections (albeit with artifacts), such a model is impractical to achieve in real-world scenarios. Images generated using a conventionally recoverable smoothed background model are substantially compromised. Statistical imaging, however, shows great promise in significantly improving and recovering reflectors, provided the statistical parameters for generating velocity realizations are accurately estimated or guessed. This approach leverages the statistical properties of the clutter to create ensembles of velocity models, allowing for more effective phase cleanup and improved imaging. Our heuristic explanation, building on concepts from speckle noise studies, elucidates why statistical imaging works for near-surface scenarios with small-scale heterogeneities.

In practical terms, statistical imaging can significantly enhance the clarity and accuracy of subsurface images in complex near-surface environments, making it a valuable

tool for geophysical exploration. The ability to achieve accurate images without requiring an exact velocity model underscores the robustness of statistical imaging, offering a practical solution where precise models are unattainable. This approach provides a feasible method for handling real-world seismic data impacted by near-surface clutter, thereby improving the reliability of seismic interpretations.

Future studies should evaluate the sensitivity of path-summation imaging to the accuracy of the statistical parameters used to characterize random heterogeneity. This will help refine the technique and enhance its robustness. Incorporating geological knowledge to assess plausible statistical properties describing near-surface geology can further improve the accuracy of statistical imaging. Advances in acoustics can aid in estimating clutter parameters in heterogeneous initial models, facilitating the creation of appropriate realizations required for the path summation approach. Additionally, further research should explore the intersection of statistical imaging with uncertainty quantification of complex velocity models, enhancing the reliability of seismic data interpretations. The main limitation of the statistical imaging is loose of high frequencies due to attenuation upon stacking. Despite of that, the potential to recover higher frequencies in the future holds promise for further improving imaging quality.

In summary, statistical imaging with path summation presents a powerful alternative to traditional deterministic methods, offering significant improvements in imaging quality for complex near-surface environments. We should emphasize that statistical imaging should provide similar results in another geological context because its ability to average out phase distortions and reveal clearer subsurface images paves the way for more accurate and reliable seismic interpretations, making it a promising area for ongoing and future research.

Acknowledgments. Authors are grateful to Saudi Aramco for the support and for the permission to publish the results. Authors are grateful to Evgeny Landa for inspiring discussions. This work is partially supported by the Russian Science Foundation within the framework of the project № 21-71-20002-П: Maxim Protasov provides realistic models using statistical modeling.

Disclosure of Interests. The authors have no competing interests to declare that are relevant to the content of this article.

References

1. Bakulin, A., Neklyudov, D., Silvestrov, I.: Importance of phase guides from beamformed data for processing multi-channel data in highly scattering media. J. Acoust. Soc. Am. Express Lett. **147**(6), EL447–EL552 (2020)
2. Xie, X.-B., Ning, H., Chen, B.: How scatterings from small-scale near-surface heterogeneities affecting seismic data and the quality of depth image, analysis based on seismic resolution. In: SEG Technical Program Expanded Abstracts, pp. 4278–4282. SEG (2016)
3. Ikelle, L.T., Yung, S.K., Daube, F.: 2-D random media with ellipsoidal autocorrelation functions. Geophysics **58**, 1359–1372 (1993)
4. Borcea, L., Papanicolaou, G., Tsogka, C.: Theory and applications of time reversal and interferometric imaging. Inverse Prob. **19**, S139–S164 (2003)

5. Sava, P., Poliannikov, O.: Interferometric imaging condition for wave-equation migration. Geophysics **73**, S47–S61 (2008)
6. Landa, E., Fomel, S., Moser, T.J.: Path-integral seismic imaging. Geophys. Prospect. **54**, 491–503 (2006)
7. Landa, E.: Imaging without a velocity model using pathsummation approach. In: SEG Technical Program Expanded Abstracts, pp. 1016–1019. SEG (2004)
8. Keydar, S., Shtivelman, V.: Imaging zero-offset sections using multipath summation. First Break **23**, 21–24 (2005)
9. Yilmaz, Ö.: Circumventing velocity uncertainty in imaging complex structures. Lead. Edge **37**, 14–18 (2018)
10. Schleicher, J., Costa J.C.: Migration velocity analysis by double path-integral migration. Geophysics **74**, WCA225–WCA231 (2009)
11. Burnett, W., Fomel, S., Bansal, R.: Diffraction velocity analysis by path-integral seismic imaging. In: SEG Technical Program Expanded Abstracts, pp. 3898–3902. SEG (2011)
12. Decker, L., Fomel S., Path-integral seismic diffraction imaging with probability weights. In: SEG Technical Program Expanded Abstracts, pp. 4231–4235. SEG (2019)
13. Protasov, M., Kolyukhin, D., Rostomyan, S., Landa, E.: Subsalt imaging in the presence of salt-body uncertainty. Lead. Edge **2**, 146–150 (2017)
14. Pyrak-Nolte, L.: Seismic imaging of fractured media. In: 5th International Workshop on the Application of Geophysics in Rock Engineering, pp. 5–13 (2002)
15. Goodman, J.W.: Speckle Phenomena in Optics: Theory and Applications. Roberts & Company (2007)
16. Bakulin, A., Neklyudov, D., Silvestrov, I.: Multiplicative seismic noise caused by small-scale near-surface scattering and its transformation during stacking. Geophysics **87**(5), V419–V435 (2022)